

Energy spectra of gamma rays, electrons, and neutrinos produced at interactions of relativistic protons with low energy radiation

S. R. Kelner^{1,2,*} and F. A. Aharonian^{2,3,+}¹*Moscow Institute of Engineering Physics, Kashirskoe sh. 31, Moscow, 115409 Russia*²*Max-Planck-Institut für Kernphysik, Saupfercheckweg 1, D-6917 Heidelberg, Germany*³*Dublin Institute for Advanced Studies, 31 Fitzwilliam Place, Dublin 2, Ireland*

(Received 5 March 2008; published 14 August 2008)

We derived simple analytical parametrizations for energy distributions of photons, electrons, and neutrinos produced in interactions of relativistic protons with an isotropic monochromatic radiation field. The results on photomeson processes are obtained using numerical simulations of proton-photon interactions based on the public available Monte Carlo code SOPHIA. For calculations of energy spectra of electrons and positrons from the pair-production (Bethe-Heitler) process we suggest a simple formalism based on the well-known differential cross section of the process in the rest frame of the proton. The analytical presentations of energy distributions of photons and leptons provide a simple but accurate approach for calculations of broadband energy spectra of gamma rays and neutrinos in cosmic proton accelerators located in radiation dominated environments.

DOI: [10.1103/PhysRevD.78.034013](https://doi.org/10.1103/PhysRevD.78.034013)

PACS numbers: 12.20.Ds, 13.20.Cz, 13.60.-r, 13.85.Qk

I. INTRODUCTION

In astrophysical environments the density of low energy radiation often exceeds the density of the gas component. Under such conditions, the interactions of ultrarelativistic protons and nuclei with radiation can dominate over interactions with the ambient gas. These interactions proceed through three channels: (i) inverse Compton scattering, $p\gamma \rightarrow p\gamma'$, (ii) electron-positron pair production, $p + \gamma \rightarrow pe^+e^-$, and (iii) photomeson production, $p\gamma \rightarrow N + k\pi$. While the inverse Compton scattering does not have a kinematic threshold, the electron-positron pair production and the photomeson production processes take place when the energy of the photon in the rest frame of the projectile proton exceeds $2m_e c^2 \simeq 1$ MeV and $m_\pi c^2(1 + m_\pi/2m_p) \simeq 145$ MeV, respectively.

The process of inverse Compton scattering of protons is identical to the inverse Compton scattering of electrons, but the energy loss rate of protons is suppressed by a factor of $(m_e/m_p)^4 \approx 10^{-13}$. At energies above the threshold of production of electron-positron pairs this process is 4 orders of magnitude slower compare to the losses caused by pair production. Therefore, generally the inverse Compton scattering does not play a significant role even in extremely dense radiation fields.

The cross section of (e^+, e^-) pair production (often called the Bethe-Heitler cross section) is quite large, but only a small ($\leq 2m_e/m_p$) fraction of the proton energy is converted to the secondary electrons. The cross section of photomeson production is smaller, but instead a substantial (10% or more) fraction of the proton energy is transferred to the secondary product. As a result, when the proton

energy exceeds the π -meson production threshold, the hadronic interactions of protons dominate over the pair production.

The cross section of pair production is calculated with a very high accuracy using the standard routines of quantum electrodynamics. The cross sections of photomeson processes are provided from accelerator experiments and phenomenological studies. Generally, for astrophysical applications the data obtained in fixed target experiments with gamma-ray beams of energies from 150 MeV to 10 GeV are sufficient, especially in the case of the broadband spectra of target photons, when the hadron-photon interactions are contributed mainly from the region not far from the energy threshold of the process.

The energy losses of protons in the photon fields, in particular, in the context of interactions of highest energy cosmic rays with 2.7 K cosmic microwave background radiation (CMBR), have been comprehensively studied by many authors (see, e.g., Refs. [1–5]). Less attention has been given to calculations of the product energy distributions. This can be partly explained by the fact that the cross sections of secondary electrons and gamma rays with the ambient photons significantly exceeds the cross sections of interactions of protons with the same target photons. Therefore the electrons and gamma rays cannot leave the active regions of their production, but rather trigger electromagnetic cascades in the surrounding radiation and magnetic fields. The spectra of gamma rays formed during the cascade development are not sensitive to the initial energy distributions, and therefore simple approximate approaches (see, e.g., Ref. [6]) can provide adequate accuracies for calculations of the characteristics of optically thick sources. This does not concern, however, neutrinos which freely escape the source and thus have an undistorted imprint of parent protons. Moreover, at some spe-

*skelner@rambler.ru

+Felix.Aharonian@mpi-hd.mpg.de

cific conditions, the secondary electrons from the pair- and photomeson production processes can cool mainly through synchrotron radiation for which the source can be optically thin (see, e.g., [7–10]). Thus the exact calculations of spectra of secondary electrons are quite important, since the synchrotron radiation of these electrons carry direct information about the energy spectra of accelerated protons.

The interactions of hadrons with radiation fields can be effectively modeled by Monte Carlo simulations of characteristics of secondary products. In particular, the SOPHIA code [11] provides an adequate tool for the comprehensive study of high energy properties of hadronic sources in which interactions of ultrarelativistic protons with ambient low energy photons dominate over other processes. At the same time, it is useful to have a complementary tool for study of radiation characteristics of hadronic sources, especially when one deals with simple scenarios, e.g., interactions of protons with a homogeneous and isotropic source of radiation in which the hadronic cascades (i.e., the next generation particles) do not play an important role. Motivated by this objective, in this paper we develop a simple approach based on the description of the energy distributions of final products from the photomeson and electron-positron pair-production processes in analytical forms which can be easily integrated in any complex model of hadronic interactions in high energy astrophysical sources. To a certain extent, this paper can be considered as a continuation of our first paper [12] where we obtained analytical presentations for proton-proton interactions.

II. PHOTOMESON PROCESSES

The formation of high energy gamma rays, electrons, and neutrinos in photomeson interactions proceeds through production and decay of nonstable secondary products, mainly π^0 and π^\pm mesons:

$$\gamma + p \rightarrow n_0 \pi^0 + n_+ \pi^+ + n_- \pi^- + \dots, \quad (1)$$

where n_0 , n_+ , and n_- are the numbers of produced pions. Hereafter we will assume that the density of the ambient medium is sufficiently low, thus the pions decay before they interact with the surrounding gas, radiation, and magnetic fields. We will also assume that (i) both the relativistic protons and the target low energy photons are isotropically distributed, and (ii) the energy of colliding particles

$$\epsilon \ll m_\pi c^2, \quad E_p \gg m_p c^2, \quad (2)$$

where ϵ is the energy of the target photon, m_π is the mass of the π meson (we will assume that $m_\pi^0 = m_\pi^\pm$), and E_p and m_p are the energy and the mass of proton. Those conditions, which are always satisfied in astronomical environments, allow us to obtain simple analytical presentations for energy distributions of the final products of π decays—photons and leptons.

The total cross section of inelastic γ - p interactions is a function of the scalar $\mathcal{E}_\gamma \equiv (k \cdot p)/m_p$, where k and p are four-momenta of the photon and proton. The scalar \mathcal{E}_γ is simply the energy of the photon in the proton rest frame. The total cross section $\sigma(\mathcal{E}_\gamma)$, calculated using the routines of the code SOPHIA [11], is presented in Fig. 1. Although the production of pions dominates in the γ - p interactions, some other channels, in particular, the ones leading to production of K and η mesons, contribute noticeably (up to 10% to 20%) to the overall production of photons and leptons. These channels are taken into account in our calculations presented below. They are based on the SOPHIA code which allows simulations of all important processes belong to γ - p interactions.

A. Production of gamma rays

The inclusive cross section of production of π^0 mesons

$$d\sigma_{\pi^0} = S(\mathbf{k}, \mathbf{p}, \mathbf{p}_{\pi^0}) d^3 p_{\pi^0} \quad (3)$$

depends on the momenta \mathbf{k} , \mathbf{p} , \mathbf{p}_{π^0} of the photon, proton, and π^0 meson, respectively. Let us denote by

$$dw = W(\mathbf{p}_{\pi^0}, \mathbf{p}_\gamma) d^3 p_\gamma \quad (4)$$

the probability of decay of a π^0 meson with momentum \mathbf{p}_{π^0} into a gamma-ray photon of momentum \mathbf{p}_γ in the volume $d^3 p_\gamma$ of the momentum space. Then

$$d\sigma_\gamma = 2d^3 p_\gamma \int S(\mathbf{k}, \mathbf{p}, \mathbf{p}_{\pi^0}) W(\mathbf{p}_{\pi^0}, \mathbf{p}_\gamma) d^3 p_{\pi^0} \quad (5)$$

can be treated as the inclusive cross section of γ -rays production through the chain $\gamma + p \rightarrow n_0 \pi^0 + \dots \rightarrow 2n_0 \gamma + \dots$.

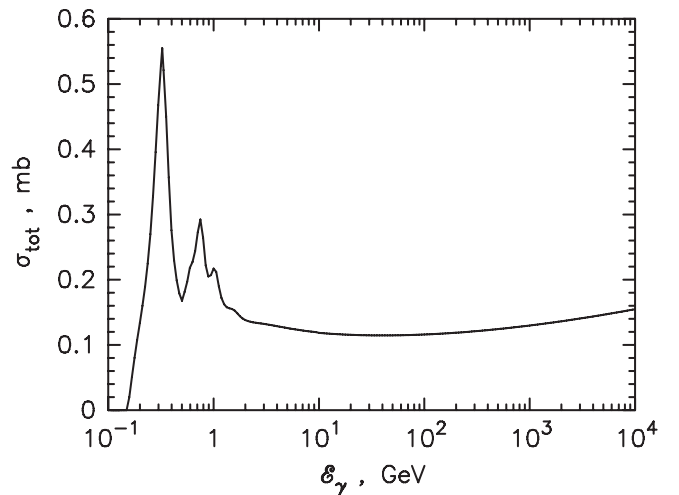


FIG. 1. The total cross section of the inelastic γ - p interactions as a function of energy of the gamma ray in the proton rest frame. The calculations have been performed using the routine of the code SOPHIA [11].

For isotropic distributions of initial particles, the final products will be isotropically distributed as well. Therefore for the determination of the energy spectra of gamma rays we can use the inclusive cross section given by Eq. (5) but integrated over the gamma-rays emission angles:

$$d\sigma_\gamma \equiv G_\gamma(E_p, \epsilon, \cos\theta, E_\gamma) \frac{dE_\gamma}{E_p}. \quad (6)$$

The function G_γ depends on E_p , ϵ , E_γ , and the angle θ between the momenta of colliding proton and photon. The corresponding differential interaction rate is

$$dw_\gamma = c(1 - \cos\theta)G_\gamma(E_p, \epsilon, \cos\theta, E_\gamma) \frac{dE_\gamma}{E_p}. \quad (7)$$

Let $f_p(E_p)$ and $f_{\text{ph}}(\epsilon)$ be functions characterizing the energy distributions of initial protons and photons, i.e., $f_p(E_p)dE_p$ and $f_{\text{ph}}(\epsilon)d\epsilon$ are the numbers of protons and photons per 1 cm³ in the energy intervals dE_p and $d\epsilon$, respectively. Since it is assumed that the target photons are isotropically distributed, their angular distribution is described as $d\Omega/4\pi$. Then the production rate of gamma rays (i.e., the number of gamma rays in the energy interval $(E_\gamma, E_\gamma + dE_\gamma)$ per sec, per 1 cm³) can be obtained after integration of Eq. (7) over energies of protons and target photons, as well as over the solid angle $d\Omega$:

$$dN_\gamma(E_\gamma) = dE_\gamma \int \frac{dE_p}{E_p} \frac{d\Omega}{4\pi} d\epsilon f_p(E_p) f_{\text{ph}}(\epsilon) c(1 - \cos\theta) \times G_\gamma(E_p, \epsilon, \cos\theta, E_\gamma). \quad (8)$$

Let us introduce the function Φ_γ defined as

$$\Phi_\gamma(\eta, x) \equiv \int c(1 - \cos\theta)G_\gamma(E_p, \epsilon, \cos\theta, E_\gamma) \frac{d\Omega}{4\pi}, \quad (9)$$

where

$$\eta = \frac{4\epsilon E_p}{m_\pi^2 c^4}, \quad x = \frac{E_\gamma}{E_p}. \quad (10)$$

Then Eq. (8) can be written in the following form:

$$\frac{dN_\gamma}{dE_\gamma} = \int f_p(E_p) f_{\text{ph}}(\epsilon) \Phi_\gamma(\eta, x) \frac{dE_p}{E_p} d\epsilon. \quad (11)$$

Note that Φ_γ can be treated as a function of two (but not three) variables. This is connected with the fact that, as we assume, at $E_p \rightarrow \infty$ and $\epsilon \rightarrow 0$, $E_\gamma \rightarrow \infty$, and for fixed x and η , the function Φ_γ should have a certain limit. In other words, at the rescaling

$$E_p \rightarrow \lambda E_p \quad E_\gamma \rightarrow \lambda E_\gamma, \quad \epsilon \rightarrow \epsilon/\lambda, \quad (12)$$

where λ is an arbitrary number ($\lambda > 1$), the function Φ_γ is not changed, therefore the following relation takes place:

$$\begin{aligned} & \int (1 - \cos\theta) G_\gamma(\lambda E_p, \epsilon/\lambda, \cos\theta, \lambda E_\gamma) d\Omega \\ &= \int (1 - \cos\theta) G_\gamma(E_p, \epsilon, \cos\theta, E_\gamma) d\Omega. \end{aligned} \quad (13)$$

Numerical calculations based on the code SOPHIA [11] show that already at

$$\epsilon < 10^{-3} m_\pi c^2, \quad E_p > 10^3 m_p c^2 \quad (14)$$

the relation given by Eq. (13) is readily fulfilled.

Some features of the energy spectra of gamma rays can be understood from the analysis of the kinematics of the process. In particular, for production of a single π^0 meson the following condition should be satisfied:

$$2\epsilon E_p (1 - \beta_p \cos\theta) > (2m_\pi m_p + m_\pi^2) c^4, \quad (15)$$

where β_p is the proton speed (in units of c).

Since the protons are ultrarelativistic, we will assume $\beta_p = 1$. If the condition of Eq. (15) is not satisfied, then the interaction rate given by Eq. (7) is equal to zero. Therefore, for the case of $4\epsilon E_p \leq (2m_\pi m_p + m_\pi^2) c^4$, the function $\Phi_\gamma = 0$. The integration of Eq. (11) should be performed over the region¹

$$\eta \geq \eta_0 \equiv 2 \frac{m_\pi}{m_p} + \frac{m_\pi^2}{m_p^2} \approx 0.313. \quad (16)$$

As it follows from kinematics of production of a single pion, the energy of the latter appears within

$$E_{\pi \text{ min}} \leq E_\pi \leq E_{\pi \text{ max}}, \quad (17)$$

where

$$E_{\pi \text{ max}} = E_p x_+, \quad E_{\pi \text{ min}} = E_p x_- \quad (18)$$

are the maximum and minimum energies, respectively, with

$$x_\pm = \frac{1}{2(1 + \eta)} [\eta + r^2 \pm \sqrt{(\eta - r^2 - 2r)(\eta - r^2 + 2r)}], \quad (19)$$

where $r = m_\pi/m_p \approx 0.146$.

Let us consider now the general case when the total mass of particles produced in proton-photon interactions is $M + m_\pi$. For example, the single-pion production implies $M = m_p$, while in the case of two-pion production $M = m_p + m_\pi$, etc. In this case the maximum and minimum energies of pions are

$$\tilde{E}_{\pi \text{ max}} = E_p \tilde{x}_+, \quad \tilde{E}_{\pi \text{ min}} = E_p \tilde{x}_-, \quad (20)$$

with

¹For determination of the region allowed by kinematics, we will assume $m_{\pi^\pm} = m_{\pi^0} = 0.137$ GeV. Since on the border of this region the function $\Phi_\gamma = 0$, this approximation does not affect the accuracy of numerical calculations.

$$\tilde{x}_{\pm} = \frac{1}{2(1+\eta)}[\eta + r^2 + 1 - R^2 \pm \sqrt{(\eta + 1 - (R+r)^2)(\eta + 1 - (R-r)^2)}], \quad (21)$$

where $R = M/m_p$. In particular, for $R = 1$, Eqs. (19) and (21) coincide. For $R > 1$, we have the following inequalities:

$$E_{\pi \min} < \tilde{E}_{\pi \min}, \quad E_{\pi \max} > \tilde{E}_{\pi \max}. \quad (22)$$

The decay of ultrarelativistic π^0 mesons with energy distribution $J_{\pi}(E_{\pi})$ within the limits given by Eq. (17), results in the energy spectrum of gamma rays

$$\frac{dN_{\gamma}}{dE_{\gamma}} = 2 \int_{E_1}^{E_{\pi \max}} \frac{dE_{\pi}}{E_{\pi}} J_{\pi}(E_{\pi}), \quad (23)$$

where

$$E_1 = \max\left(E_{\gamma}, \frac{m_{\pi}^2 c^4}{4E_{\gamma}}, E_{\pi \min}\right), \quad E_{\gamma} < E_{\pi \max}. \quad (24)$$

Below we will be interested in gamma rays with energy $E_{\gamma} > m_{\pi}/2$. While in the energy range $E_{\gamma} < E_{\pi \min}$, the differential spectrum of gamma rays is flat,

$$\frac{dN_{\gamma}}{dE_{\gamma}} = 2 \int_{E_{\pi \min}}^{E_{\pi \max}} \frac{dE_{\pi}}{E_{\pi}} J_{\pi}(E_{\pi}), \quad (25)$$

within the interval $E_{\pi \min} < E_{\gamma} < E_{\pi \max}$ the spectrum decreases with energy,

$$\frac{dN_{\gamma}}{dE_{\gamma}} = 2 \int_{E_{\gamma}}^{E_{\pi \max}} \frac{dE_{\pi}}{E_{\pi}} J_{\pi}(E_{\pi}). \quad (26)$$

The above quantitative features of the spectrum of gamma rays appear quite useful for the choice of approximate analytical presentations. The results of numerical calculations of the function Φ_{γ} based on simulations using the code SOPHIA [11] can be approximated, with an accuracy better than 10% by simple analytical formulas. Namely, in the range $x_- < x < x_+$

$$\Phi_{\gamma}(\eta, x) = B_{\gamma} \exp\left\{-s_{\gamma} \left[\ln\left(\frac{x}{x_-}\right)\right]^{\delta_{\gamma}}\right\} \times \left[\ln\left(\frac{2}{1+y^2}\right)\right]^{2.5+0.4 \ln(\eta/\eta_0)}, \quad (27)$$

where

$$y = \frac{x - x_-}{x_+ - x_-}. \quad (28)$$

At low energies, $x < x_-$, the spectrum does not depend on x ,

$$\Phi_{\gamma}(\eta, x) = B_{\gamma} (\ln 2)^{2.5+0.4 \ln(\eta/\eta_0)}. \quad (29)$$

Finally in the range $x > x_+$, the function $\Phi_{\gamma} = 0$.

All three parameters B_{γ} , s_{γ} , and δ_{γ} used in this presentation are functions of η . The numerical values of these parameters are shown in Table I. At $\eta/\eta_0 = 1$, i.e., at the threshold of π^0 -meson production, $B_{\gamma} = 0$. In Fig. 2 we show the functions $x\Phi_{\gamma}(\eta, x)$ obtained with the code SOPHIA (histograms) and the analytical presentations given by Eqs. (27) and (29) for two values of η .

Equation (11) provides a simple approach for calculations of gamma-ray spectra for arbitrary energy distributions of ultrarelativistic protons and ambient photons. The parameters B_{γ} , s_{γ} , and δ_{γ} are quite smooth functions of η ; thus for calculations of these parameters at intermediate values of η one can use linear interpolations of the numerical results presented in Table I. Note that for interactions of protons with 2.7 K CMBR, the results presented in Table I allow calculations of gamma-ray spectra up to $\sim 10^{21}$ eV.

B. Production of electrons and neutrinos

The production of leptons in proton-photon interactions is dominated by the decay of secondary charged pions. In analogy with Eq. (11), the spectrum of each type of leptons can be presented in the form

$$N_l(E_l) dE_l = dE_l \int f_p(E_p) f_{\text{ph}}(\epsilon) \Phi_l(\eta, x) \frac{dE_p}{E_p} d\epsilon, \quad (30)$$

where η is determined in Eq. (10), $x = E_l/E_p$, and l

TABLE I. Numerical values of parameters B_{γ} , s_{γ} , and δ_{γ} characterizing the gamma-ray spectra given by Eq. (11).

η/η_0	s_{γ}	δ_{γ}	$B_{\gamma}, \text{cm}^3/\text{s}$
1.1	0.0768	0.544	2.86×10^{-19}
1.2	0.106	0.540	2.24×10^{-18}
1.3	0.182	0.750	5.61×10^{-18}
1.4	0.201	0.791	1.02×10^{-17}
1.5	0.219	0.788	1.60×10^{-17}
1.6	0.216	0.831	2.23×10^{-17}
1.7	0.233	0.839	3.10×10^{-17}
1.8	0.233	0.825	4.07×10^{-17}
1.9	0.248	0.805	5.30×10^{-17}
2.0	0.244	0.779	6.74×10^{-17}
3.0	0.188	1.23	1.51×10^{-16}
4.0	0.131	1.82	1.24×10^{-16}
5.0	0.120	2.05	1.37×10^{-16}
6.0	0.107	2.19	1.62×10^{-16}
7.0	0.102	2.23	1.71×10^{-16}
8.0	0.0932	2.29	1.78×10^{-16}
9.0	0.0838	2.37	1.84×10^{-16}
10.0	0.0761	2.43	1.93×10^{-16}
20.0	0.107	2.27	4.74×10^{-16}
30.0	0.0928	2.33	7.70×10^{-16}
40.0	0.0772	2.42	1.06×10^{-15}
100.0	0.0479	2.59	2.73×10^{-15}

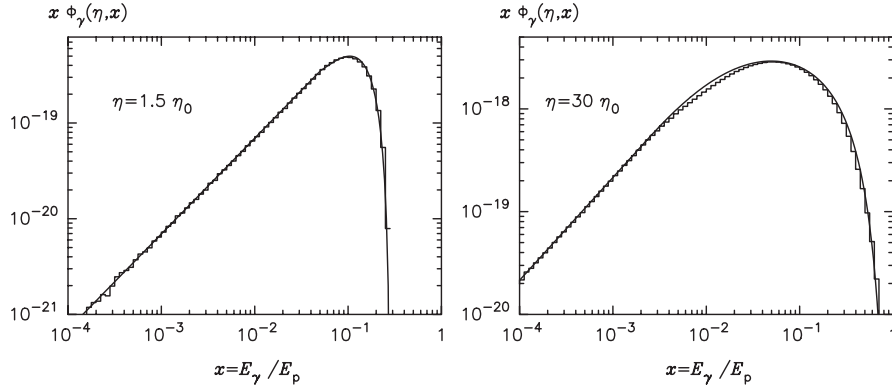


FIG. 2. Gamma-ray spectra produced in photomeson interactions calculated for two values of $\eta = 4\epsilon E_p/m_p^2 c^4$. Solid lines are calculated using the analytical presentations given by Eq. (11), and the histograms are from simulations using the SOPHIA code.

implies one of the following symbols: e^+ , e^- , ν_μ , $\bar{\nu}_\mu$, ν_e , or $\bar{\nu}_e$.

As in the case of gamma rays, the energy range of leptons, for the fixed values of E_p and ϵ , is determined by kinematics. We obtained analytical forms for the energy spectra for all lepton types, Φ_l , using numerical results of simulations of the SOPHIA code. In the range of $x'_- < x < x'_+$

$$\Phi_l(\eta, x) = B_l \exp\left\{-s_l \left[\ln\left(\frac{x}{x'_-}\right)\right]^{\delta_l}\right\} \left[\ln\left(\frac{2}{1+y'^2}\right)\right]^\psi, \quad (31)$$

where

$$y' = \frac{x - x'_-}{x'_+ - x'_-}. \quad (32)$$

In range of $x < x'_-$, the function Φ_l does not depend on x :

$$\Phi_l(\eta, x) = B_l (\ln 2)^\psi. \quad (33)$$

For $x \geq x'_+$, the function $\Phi_l = 0$. The analytical presentation in the form of Eq. (31) contains three parameters s_l , δ_l , and B_l which themselves are functions of η . The numerical values of these parameters obtained with the method of least squares are tabulated in Table II (for e^+ , $\bar{\nu}_\mu$, ν_μ , and ν_e) and Table III (for e^- and $\bar{\nu}_e$). The values of x'_\pm and ψ are given below for each type of leptons.

TABLE II. Numerical values of parameters s_l , δ_l , and B_l for e^+ , $\bar{\nu}_\mu$, ν_μ , and ν_e .

η/η_0	s_{e^+}	δ_{e^+}	$B_{e^+}, \text{cm}^3/\text{s}$	$s_{\bar{\nu}_\mu}$	$\delta_{\bar{\nu}_\mu}$	$B_{\bar{\nu}_\mu}, \text{cm}^3/\text{s}$	s_{ν_μ}	δ_{ν_μ}	$B_{\nu_\mu}, \text{cm}^3/\text{s}$	s_{ν_e}	δ_{ν_e}	$B_{\nu_e}, \text{cm}^3/\text{s}$
1.1	0.367	3.12	8.09×10^{-19}	0.365	3.09	8.09×10^{-19}	0.0	0.0	1.08×10^{-18}	0.768	2.49	9.43×10^{-19}
1.2	0.282	2.96	7.70×10^{-18}	0.287	2.96	7.70×10^{-18}	0.0778	0.306	9.91×10^{-18}	0.569	2.35	9.22×10^{-18}
1.3	0.260	2.83	2.05×10^{-17}	0.250	2.89	1.99×10^{-17}	0.242	0.792	2.47×10^{-17}	0.491	2.41	2.35×10^{-17}
1.4	0.239	2.76	3.66×10^{-17}	0.238	2.76	3.62×10^{-17}	0.377	1.09	4.43×10^{-17}	0.395	2.45	4.20×10^{-17}
1.5	0.224	2.69	5.48×10^{-17}	0.220	2.71	5.39×10^{-17}	0.440	1.06	6.70×10^{-17}	0.31	2.45	6.26×10^{-17}
1.6	0.207	2.66	7.39×10^{-17}	0.206	2.67	7.39×10^{-17}	0.450	0.953	9.04×10^{-17}	0.323	2.43	8.57×10^{-17}
1.7	0.198	2.62	9.52×10^{-17}	0.197	2.62	9.48×10^{-17}	0.461	0.956	1.18×10^{-16}	0.305	2.40	1.13×10^{-16}
1.8	0.193	2.56	1.20×10^{-16}	0.193	2.56	1.20×10^{-16}	0.451	0.922	1.32×10^{-16}	0.285	2.39	1.39×10^{-16}
1.9	0.187	2.52	1.47×10^{-16}	0.187	2.52	1.47×10^{-16}	0.464	0.912	1.77×10^{-16}	0.270	2.37	1.70×10^{-16}
2.0	0.181	2.49	1.75×10^{-16}	0.178	2.51	1.74×10^{-16}	0.446	0.940	2.11×10^{-16}	0.259	2.35	2.05×10^{-16}
3.0	0.122	2.48	3.31×10^{-16}	0.123	2.48	3.38×10^{-16}	0.366	1.49	3.83×10^{-16}	0.158	2.42	3.81×10^{-16}
4.0	0.106	2.50	4.16×10^{-16}	0.106	2.56	5.17×10^{-16}	0.249	2.03	5.09×10^{-16}	0.129	2.46	4.74×10^{-16}
5.0	0.0983	2.46	5.57×10^{-16}	0.0944	2.57	7.61×10^{-16}	0.204	2.18	7.26×10^{-16}	0.113	2.45	6.30×10^{-16}
6.0	0.0875	2.46	6.78×10^{-16}	0.0829	2.58	9.57×10^{-16}	0.174	2.24	9.26×10^{-16}	0.0996	2.46	7.65×10^{-16}
7.0	0.0830	2.44	7.65×10^{-16}	0.0801	2.54	1.11×10^{-15}	0.156	2.28	1.07×10^{-15}	0.0921	2.46	8.61×10^{-16}
8.0	0.0783	2.44	8.52×10^{-16}	0.0752	2.53	1.25×10^{-15}	0.140	2.32	1.19×10^{-15}	0.0861	2.45	9.61×10^{-16}
9.0	0.0735	2.45	9.17×10^{-16}	0.0680	2.56	1.36×10^{-15}	0.121	2.39	1.29×10^{-15}	0.0800	2.47	1.03×10^{-15}
10.0	0.0644	2.50	9.57×10^{-16}	0.0615	2.60	1.46×10^{-15}	0.107	2.46	1.40×10^{-15}	0.0723	2.51	1.10×10^{-15}
30.0	0.0333	2.77	3.07×10^{-15}	0.0361	2.78	5.87×10^{-15}	0.0705	2.53	5.65×10^{-15}	0.0411	2.70	3.55×10^{-15}
100.0	0.0224	2.86	1.58×10^{-14}	0.0228	2.88	3.10×10^{-14}	0.0463	2.62	3.01×10^{-14}	0.0283	2.77	1.86×10^{-14}

TABLE III. Numerical values of parameters s_l , δ_l , and B_l for electrons and electron antineutrinos.

η/η_0	s_{e^-}	δ_{e^-}	$B_{e^-}, \text{cm}^3/\text{s}$	$s_{\bar{\nu}_e}$	$\delta_{\bar{\nu}_e}$	$B_{\bar{\nu}_e}, \text{cm}^3/\text{s}$
3.0	0.658	3.09	6.43×10^{-19}	0.985	2.63	6.61×10^{-19}
4.0	0.348	2.81	9.91×10^{-18}	0.378	2.98	9.74×10^{-18}
5.0	0.286	2.39	1.24×10^{-16}	0.31	2.31	1.34×10^{-16}
6.0	0.256	2.27	2.67×10^{-16}	0.327	2.11	2.91×10^{-16}
7.0	0.258	2.13	3.50×10^{-16}	0.308	2.03	3.81×10^{-16}
8.0	0.220	2.20	4.03×10^{-16}	0.292	1.98	4.48×10^{-16}
9.0	0.217	2.13	4.48×10^{-16}	0.260	2.02	4.83×10^{-16}
10.0	0.192	2.19	4.78×10^{-15}	0.233	2.07	5.13×10^{-16}
30.0	0.125	2.27	1.64×10^{-15}	0.135	2.24	1.75×10^{-15}
100.0	0.0507	2.63	4.52×10^{-15}	0.0770	2.40	5.48×10^{-15}

I. Energy spectra of positrons, muon antineutrinos, and electron neutrinos

For e^+ , $\bar{\nu}_\mu$, and ν_e , the parameter ψ is presented in the form

$$\psi = 2.5 + 1.4 \ln\left(\frac{\eta}{\eta_0}\right), \quad (34)$$

with

$$x'_- = \frac{x_-}{4} \quad \text{and} \quad x'_+ = x_+, \quad (35)$$

where x_+ and x_- are determined from Eq. (19); η_0 is defined in Eq. (16). Note that here ψ is different than the relevant function in Eq. (27). In Figs. 3 and 4 the analytical presentations of distributions $x\Phi_{e^+}$ and $x\Phi_{\bar{\nu}_\mu}$ are compared with Monte Carlo simulations based on the SOPHIA code.

In the range

$$\eta < 4 \frac{m_\pi}{m_p} + 4 \left(\frac{m_\pi}{m_p}\right)^2 = 2.14\eta_0,$$

only a single π^+ meson can be produced. It decays to $\pi^+ \rightarrow \mu^+ \nu_\mu$. The positrons and muon antineutrinos are produced from the decay $\mu^+ \rightarrow e^+ \bar{\nu}_\mu \nu_e$. Since the spectra

of e^+ and $\bar{\nu}_\mu$ from the decay of μ^+ coincide (see, e.g., [13]), the parameters in Table II calculated for e^+ and $\bar{\nu}_\mu$ for small η should be identical. The slight difference at $\eta < 2\eta_0$ is explained by fluctuations related to the statistical character of simulations.

At $\eta > 2.14\eta_0$, a new channel is opened for production of $\bar{\nu}_\mu$, because of the production of π^- mesons and their decay $\pi^- \rightarrow \mu^- \bar{\nu}_\mu$. Therefore, for large values of η , the parameters characterizing e^+ and $\bar{\nu}_\mu$ differ significantly (see Table II). This can be seen from the comparison of results presented in the right panels of Figs. 3 and 4; for $\eta = 30$, $x\Phi_{\bar{\nu}_\mu}$ significantly exceeds $x\Phi_{e^+}$.

2. Muon neutrinos

The distribution for ν_μ is described by Eq. (34) with the same function ψ as for e^+ , $\bar{\nu}_\mu$, and ν_e , given by Eq. (34), but with different parameters x'_\pm :

$$x'_+ = \begin{cases} 0.427x_+, & \rho < 2.14, \\ (0.427 + 0.0729(\rho - 2.14))x_+, & 2.14 < \rho < 10, \\ x_+, & \rho > 10, \end{cases} \quad (36)$$

where $\rho = \eta/\eta_0$, and

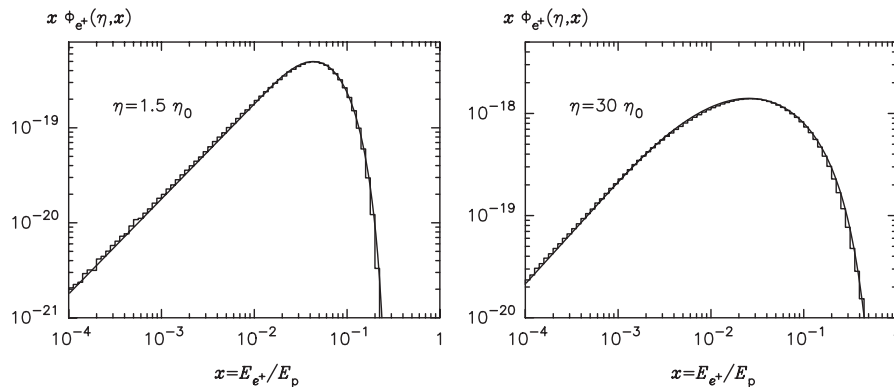


FIG. 3. Energy spectra of positrons produced in photomeson interactions calculated for two values of $\eta = 4\epsilon E_p/m_p^2 c^4$. Solid lines are calculated using the analytical presentations, and the histograms are from Monte Carlo simulations using the SOPHIA code.

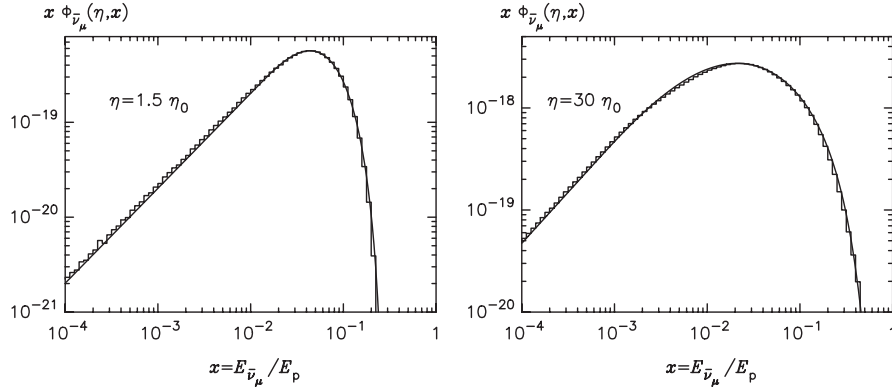


FIG. 4. The same as in Fig. 3 but for muon antineutrinos.

$$x'_- = 0.427x_- \quad (37)$$

The difference of values of x_{\pm} for $\bar{\nu}_{\mu}$ and ν_{μ} appears for the following reason. At the decay $\pi^+ \rightarrow \mu^+ \bar{\nu}_{\mu}$ the maximum energy of $\bar{\nu}_{\mu}$ is equal to $(1 - m_{\mu}^2/m_{\pi}^2)E_{\pi} \approx 0.427E_{\pi}$, where m_{μ} is the mass of the muon. On the other hand, the maximum energy of $\bar{\nu}_{\mu}$, produced at the decay of the muon is equal to E_{π} . With an increase of the parameter η , π^- mesons start to be produced, the decay of which leads to ν_{μ} , with maximum energy comparable to the energy of the pion (a detailed discussion of these questions can be found in [12]).

In Fig. 5 the function $x\Phi_{\nu_{\mu}}(\eta, x)$ is shown. The histograms are from Monte Carlo simulations using the SOPHIA code, and the solid lines correspond to the analytical approximations.

3. Electrons and electron antineutrinos

The electrons and electron antineutrinos are produced through the decay μ^- , which in its turn is a product of the decay of the π^- meson. Therefore, for production of e^- and $\bar{\nu}_e$, at least two pions should be produced. The production of two pions is energetically allowed if

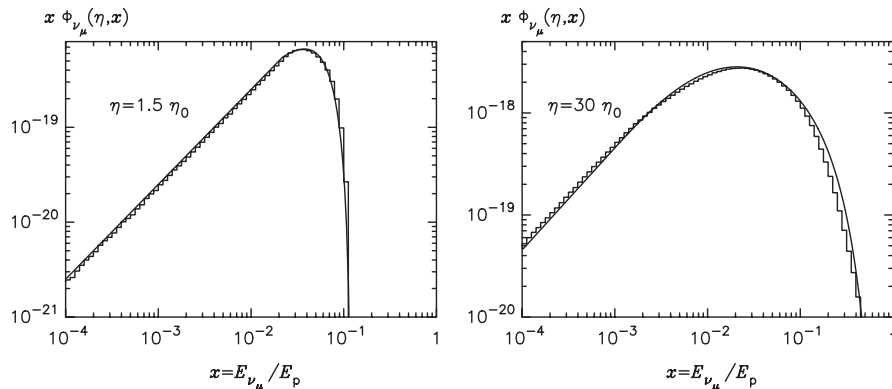


FIG. 5. The same as in Fig. 3 but for muon neutrinos.

$$\eta > \eta''_{\min} = 4r(1+r) \approx 2.14\eta_0 \quad (38)$$

The maximum and minimum energies of the pion correspondingly are

$$E'_{\pi\max} = x'_+ E_p, \quad E_{\pi\min} = x'_- E_p, \quad (39)$$

where

$$x'_{\pm} = \frac{1}{2(1+\eta)} (\eta - 2r \pm \sqrt{\eta(\eta - 4r(1+r))}). \quad (40)$$

Equation (40) is obtained from Eq. (21) if one sets $R = 1 + r$. These functions together with

$$\psi = 6(1 - e^{1.5(4-\rho)})\Theta(\rho - 4), \quad \rho = \frac{\eta}{\eta_0}, \quad (41)$$

determine the distributions for e^- and $\bar{\nu}_e$ given in a general form by Eqs. (31)–(33); $\Theta(\rho)$ is the Heaviside function [$\Theta(\rho) = 0$ if $\rho < 0$ and $\Theta(\rho) = 1$ if $\rho \geq 0$].

III. PHOTONS AND LEPTONS PRODUCED AT INTERACTIONS OF PROTONS WITH 2.7 K CMRB

In this section we compare the energy spectra of gamma rays, neutrinos, and electrons produced at photomeson interactions. For monoenergetic protons interacting with

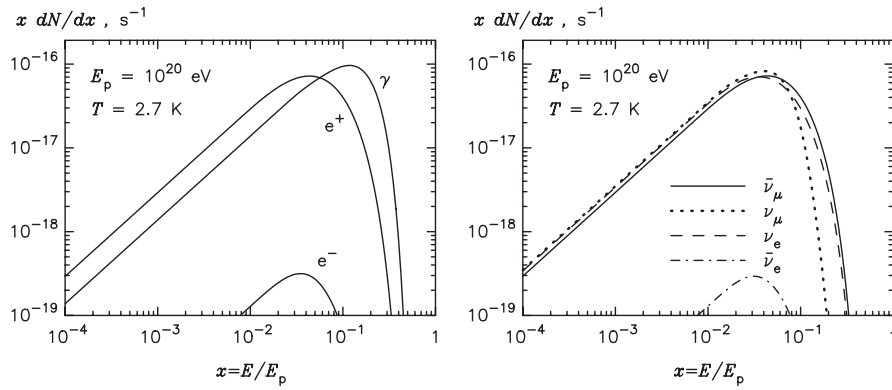


FIG. 6. The energy spectra of stable products of photomeson interactions of a proton of energy $E_p = 10^{20}$ eV with the 2.7 K CMBR. Left panel—gamma rays, electrons, and positrons; right panel—electron and muon neutrinos and antineutrinos.

a radiation field with energy distribution $f_{\text{ph}}(\epsilon)$, the energy spectra of photons and leptons can be reduced to the calculation of a one-dimensional integral

$$\frac{dN}{dx} = \int_{\epsilon_0}^{\infty} f_{\text{ph}}(\epsilon) \Phi(\eta, x) d\epsilon, \quad (42)$$

where $\epsilon_0 = \eta_0 m_p^2 c^4 / (4E_p)$, and $x = E/E_p$ is the fraction of energy of the protons transferred to the given type of secondary particle; Φ is one of the functions described in the previous section.

In Figs. 6 and 7 we show the energy spectra of gamma rays and electrons (left panels) and all neutrino types (right panels) produced by protons of energy 10^{20} and 10^{21} eV interacting with blackbody radiation of temperature $T = 2.7$ K. The results depend only on the product $E_p \times T$; therefore they can be easily rescaled to a blackbody radiation of an arbitrary temperature. The chosen radiation field and proton energies are of great practical interest in the context of origin and intergalactic propagation of ultrahigh energy cosmic rays. Because of interactions with the intergalactic radiation fields, ultrahigh energy gamma rays achieve the observer from distances less than 1 Mpc (see, e.g., Ref. [14]). The electrons rapidly cool via synchrotron radiation or, in the case of very small intergalactic mag-

netic field, initiate electromagnetic cascades supported by interactions of electrons and gamma rays with the 2.7 K CMBR. Only neutrinos freely penetrate through intergalactic radiation and magnetic fields and thus carry a clear imprint of parent protons.

In Fig. 8 we show the average number of secondaries (multiplicity) produced in one inelastic interaction of protons with 2.7 K CMBR as a function of proton energy. The results of numerical calculations are obtained using the energy spectra of secondary photons, electrons, and neutrinos, and the total cross section shown in Fig. 1. Note that below the threshold of production of two pions one should have the following relations:

$$\frac{1}{2} \langle n_{\gamma} \rangle + \langle n_{e^+} \rangle = 1, \quad \langle n_{e^+} \rangle = \langle n_{\bar{\nu}_{\mu}} \rangle = \langle n_{\nu_{\mu}} \rangle. \quad (43)$$

The results of calculations based on approximate analytical presentations of functions Φ_l satisfy these relations with an accuracy of better than 5%.

Note that at very low energies the average number of gamma rays $\langle n_{\gamma} \rangle$ appears smaller than the average number of positrons $\langle n_{e^+} \rangle$. This, at first glance, unexpected result is actually a direct consequence of the experimental fact that near the threshold the total cross section σ_{π^+} of π^+ production significantly exceeds σ_{π^0} (see Fig. 9).

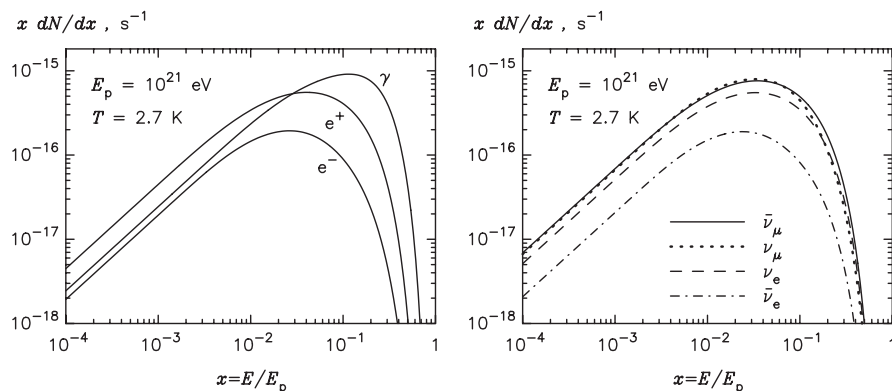


FIG. 7. The same as in Fig. 3, but for a proton of energy $E_p = 10^{21}$ eV.

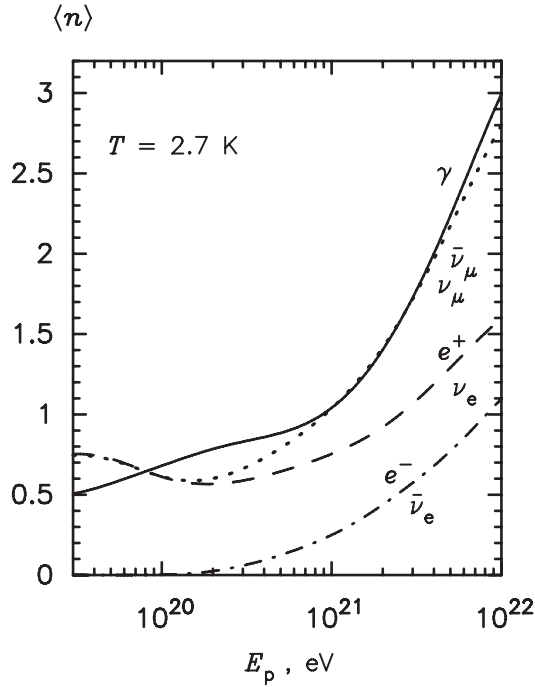


FIG. 8. The multiplicity of photons and leptons produced in one interaction of a relativistic proton with 2.7 CMBR.

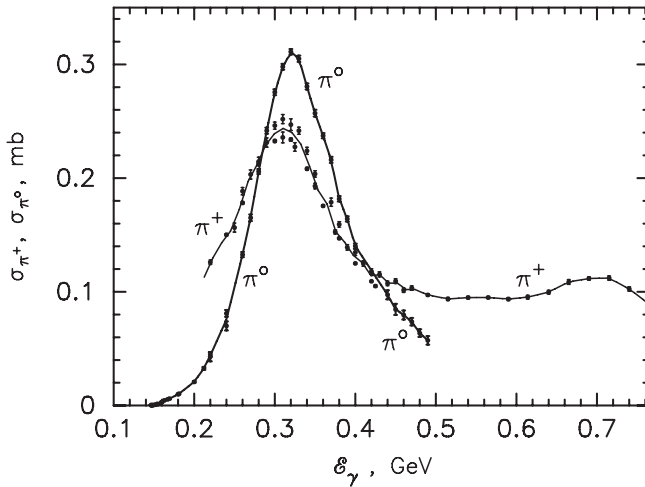


FIG. 9. The total cross sections of production of π^+ and π^0 mesons as a function of energy of the incident gamma ray in the rest frame of a proton. The experimental points are taken from <http://wwwppds.ihep.su:8001>.

IV. PRODUCTION OF ELECTRON-POSITRON PAIRS

At energies below the photomeson production, the main channel of inelastic interactions for protons with ambient photons proceeds through the direct production of electron-positron pairs. In the rest frame of the proton, this process is described by the so-called Bethe-Heitler cross section. In astrophysical environments, the process

is more often realized when ultrarelativistic protons collide with low energy photons,

$$p + \gamma \rightarrow e^+ + e^- + p. \quad (44)$$

The process is energetically allowed when

$$\gamma_p \epsilon > m_e c^2, \quad (45)$$

where $\gamma_p = E_p/m_p c^2$ is the proton Lorentz factor, ϵ is the soft photon energy, and m_e is the mass of electron. The maximum energy of the electron (positron) is determined by the kinematics of the process

$$E_{e \max} = \frac{\gamma_p}{1 + 4\gamma_p \epsilon / (m_p c^2)} (\sqrt{\gamma_p \epsilon} + \sqrt{\gamma_p \epsilon - m_e c^2})^2. \quad (46)$$

This equation is valid when $\gamma_p \gg 1$ and $\epsilon \ll m_p \gamma_p c^2$. In the interval

$$m_e c^2 \ll \gamma_p \epsilon \ll m_p c^2, \quad (47)$$

the maximum electron energy is

$$E_{e \max} = 4\gamma_p^2 \epsilon. \quad (48)$$

This applies for $E_{e \max} \ll E_p$. In the limit of $\gamma_p \epsilon \gg m_p c^2$

$$E_{e \max} = m_p c^2 \gamma_p = E_p, \quad (49)$$

i.e., the whole energy of the proton is transferred to one of the electrons.

Let us denote by $d\sigma$ the differential cross section of the process. The interaction rate is

$$dw = c^3 \frac{(k \cdot p)}{\epsilon E_p} d\sigma = c^2 \frac{(k \cdot u_p)}{\epsilon \gamma_p} d\sigma, \quad (50)$$

where k and p are four-momenta of the photon and proton, $u_p = p/m_p c$ is the four-velocity of the proton, $(k \cdot p) = \epsilon E_p / c^2 - \mathbf{k} \cdot \mathbf{p}$ is the scalar product of four-vectors. Let us assume that in a unit volume we have $f_{\text{ph}}(\epsilon) d\epsilon d\Omega / 4\pi$ photons between the energy interval $(\epsilon, \epsilon + d\epsilon)$ and moving within the solid angle $d\Omega$. Then the number of interactions per unit of time is

$$N = c^2 \int d\epsilon \frac{d\Omega}{4\pi} f_{\text{ph}}(\epsilon) \frac{(k \cdot u_p)}{\epsilon \gamma_p} \int d\sigma, \quad (51)$$

where the integration is performed over all variables.

Below we perform calculations based on the following approach. If we are interested in a distribution of some variable ξ , which is a function φ of particle momenta, this distribution can be found introducing an additional δ function under the integral in Eq. (51):

$$\frac{dN}{d\xi} = c^2 \int d\epsilon \frac{d\Omega}{4\pi} f_{\text{ph}}(\epsilon) \frac{(k \cdot u_p)}{\epsilon \gamma_p} \int \delta(\xi - \varphi) d\sigma. \quad (52)$$

In particular, the energy distribution of electrons in the laboratory frame can be calculated using the following

formula:

$$\frac{dN}{dE_e} = c^2 \int d\epsilon \frac{d\Omega}{4\pi} f_{\text{ph}}(\epsilon) \frac{(k \cdot u_p)}{\epsilon \gamma_p} \times \int \delta(E_e - c(u_{lf} \cdot p_e)) d\sigma, \quad (53)$$

where u_{lf} is the four-velocity of the laboratory frame, and p_e is the four-momentum of the electron since the scalar $c(u_{lf} \cdot p_e)$ is equal to the energy of the electron in the laboratory system. The proton Lorentz factor in the laboratory system also can be considered as a relativistic invariant: $\gamma_p = (u_{lf} \cdot u_p)$.

Note that the integral

$$S \equiv \int \delta(E_e - c(u_{lf} \cdot p_e)) d\sigma \quad (54)$$

is a relativistic invariant, so it can be calculated in any frame of coordinates. The differential cross section $d\sigma$ can be written in the simplest form in the rest frame of the proton; therefore for calculations of S we will use this system of coordinate where

$$c(u_{lf} \cdot p_e) = \gamma_p(E_- - V_p p_- \cos\theta_-). \quad (55)$$

Here E_- is the energy and $p_- = \sqrt{E_-^2/c^2 - m_e^2 c^2}$ is the momentum modulus of electron in the rest frame of the proton., θ_- is the angle between the momenta of the photon and the electron. Therefore

$$S = \int d\sigma \delta(E_e - \gamma_p(E_- - V_p p_- \cos\theta_-)). \quad (56)$$

After integration over all variables, except for E_- and θ_- , the result can be written in the form

$$S = \int W(\omega, E_-, \cos\theta_-) \times \delta(E_e - \gamma_p(E_- - V_p p_- \cos\theta_-)) dE_- d(\cos\theta_-), \quad (57)$$

where

$$W(\omega, E_-, \cos\theta_-) = \frac{d^2\sigma}{dE_- d(\cos\theta_-)} \quad (58)$$

is the double-differential cross section as a function of energy and emission angle of the electron in the rest frame of the proton; $\omega = (u_p \cdot k)/(m_e c)$ is the energy of the photon the rest frame of proton in units $m_e c^2$. The function W has been derived in the Born approximation in Refs. [15,16]. The approach used in these papers describes the production of an electron-positron pair by a photon in the Coulomb field which formally corresponds to the limit $m_p \rightarrow \infty$. However, we warn the reader that there is a misprint in the cross section published in these papers; therefore we advise one to use Eq. (10) of the paper by Blumenthal [2], where the typo is fixed. Note that in

Refs. [2,15,16] the system of units is used in which $c = \hbar = m_e = 1$. Since here we cite certain equations of these papers, in this section, in order to avoid confusion, we use the same system of units.

The presence of the δ function in the integrand allows the integration over the variable $d(\cos\theta_-)$, which gives

$$S = \frac{1}{\gamma_p V_p} \int \frac{dE_-}{p_-} W(\omega, E_-, \xi), \quad (59)$$

where

$$\xi \equiv \cos\theta_- = \frac{\gamma_p E_- - E_e}{\gamma_p V_p p_-}. \quad (60)$$

After substituting Eq. (59) into Eq. (53), and using the relation

$$\omega = (u_p \cdot k) = \epsilon \gamma_p (1 - \cos\theta), \quad (61)$$

it is convenient to perform the integration over ω instead of integration over the angle. Then, for ultrarelativistic protons ($\gamma_p \gg 1$), we obtain

$$\frac{dN}{dE_e} = \frac{1}{2\gamma_p^3} \int_{((\gamma_p + E_e)^2/4\gamma_p^2 E_e)}^{\infty} d\epsilon \frac{f_{\text{ph}}(\epsilon)}{\epsilon^2} \times \int_{((\gamma_p + E_e)^2/2\gamma_p E_e)}^{2\gamma_p \epsilon} d\omega \omega \times \int_{(\gamma_p^2 + E_e^2/2\gamma_p E_e)}^{\omega^{-1}} \frac{dE_-}{p_-} W(\omega, E_-, \xi). \quad (62)$$

When substituting Eq. (60) into (62) we set $V_p = 1$, and correspondingly $\xi = (\gamma_p E_- - E_e)/(\gamma_p p_-)$. The integration limits in Eq. (62) are found from the analysis of kinematics.

In the case of monoenergetic target photon field,

$$f_{\text{ph}}(\epsilon') = C \delta(\epsilon' - \epsilon), \quad (63)$$

the energy distribution of electrons can be written in the form of the double integral

$$\frac{dN}{dE_e} = \frac{C}{2\gamma_p^3 \epsilon^2} \int_{((\gamma_p + E_e)^2/2\gamma_p E_e)}^{2\gamma_p \epsilon} d\omega \omega \times \int_{(\gamma_p^2 + E_e^2/2\gamma_p E_e)}^{\omega^{-1}} \frac{dE_-}{p_-} W(\omega, E_-, \xi),$$

with the following kinematic condition:

$$4\epsilon \gamma_p^2 E_e \geq (\gamma_p + E_e)^2. \quad (64)$$

For the important case of Planckian distribution of target photons,

$$f_{\text{ph}}(\epsilon) = \frac{1}{\pi^2} \frac{\epsilon^2}{e^{\epsilon/kT} - 1}, \quad (65)$$

the expression can be simplified. Indeed, rewriting the first term in the integrand of Eq. (62) in the form

$$d\epsilon \frac{f_{\text{ph}}(\epsilon)}{\epsilon^2} = \frac{kT}{\pi^2} d\ln(1 - e^{-\epsilon/kT}), \quad (66)$$

we can perform integration over $d\epsilon$ by parts, which after simple transformation leads to the energy spectrum of electrons in the form of a double integral

$$\frac{dN}{dE_e} = -\frac{kT}{2\pi^2\gamma_p^3} \int_{(\gamma_p+E_e)^2/2\gamma_p E_e}^{\infty} d\omega \omega \ln(1 - e^{-\omega/(2\gamma_p kT)}) \times \int_{(\gamma_p^2+E_e^2/2\gamma_p E_e)}^{\omega-1} \frac{dE_-}{P_-} W(\omega, E_-, \xi). \quad (67)$$

In the Born approximation used in [2,15,16], the energy and angular distributions of electrons and positrons are identical, and therefore Eqs. (62) and (67) do not distinguish between electrons and positrons. Let us discuss the condition of applicability of Eqs. (62) and (67). In the proton rest system, the cross section of production of an electron-positron pair by the proton and in the Coulomb potential coincide for all emission angles of pairs, when $\omega \ll m_p$. In the laboratory frame this is equivalent to the condition $\epsilon\gamma_p \ll m_p$, which, taking into account Eq. (48), can be written in the form $E_{e\text{max}} \ll E_p$. Thus, the above obtained results can be applied to production of electrons and positrons when $E_e \ll E_p$.

In Fig. 10 we show the energy distributions of electrons and positrons produced in interactions of protons of three different energies with the 2.7 K CMBR: 6.4×10^{19} eV, 10^{20} eV, and 3×10^{20} eV. Note that the energy of the

primary proton 6.4×10^{19} eV is interesting in the sense that at this energy the loss rates of protons, $E_p^{-1} dE_p/dt$, due to pair production and photomeson production are equal. The spectral energy distribution of electron and positrons from the pair-production process, $E^2 dN/dE$, has a bell-type shape with a broad maximum around $(m_e/m_p)R_p \sim 10^{-3}E_p$. This spectrum is quite different from the $dN/dE \propto E^{-7/4}$ -type energy dependence as it was hypothesized in [10]. Figure 10 demonstrates that while the low energy range of electrons (positrons) is dominated by the process of pair production, at higher energies the main contribution comes from photomeson processes. Fortunately, in the energy range where Eqs. (62) and (67) are not valid, the contribution of pair production to the spectrum of electrons is negligible compared to the contribution of photomeson processes.

It should be noted that the δ -functional approximation, which is often used for qualitative estimates of characteristics of products of high energy interactions, in this specific process does not provide adequate accuracy. The reason is that the electrons produced in a single act of interaction have very broad energy distribution. The calculations show that the δ -functional approximation leads to significant deviation from the exact result given by Eq. (62), even when one takes into account the energy dependence of the average fraction of the proton energy transferred to the electron.

A. Energy losses

The analytical presentations of the energy spectra of stable products of interactions of protons with ambient low energy photons allow us to calculate the energy losses of protons in a radiation field with arbitrary energy distribution,

$$\frac{1}{E_p} \left| \frac{dE_p}{dt} \right| = \int_0^1 dx x \int_{\epsilon_{\min}}^{\infty} d\epsilon f_{\text{ph}}(\epsilon) \Phi(\eta, x), \quad (68)$$

where $\epsilon_{\min} = \eta_0 m_p^2 c^4 / (4E_p)$, and $\Phi(\eta, x)$ is the sum of all seven energy distribution (relevant to γ , e^+ , e^- , ν_μ , $\bar{\nu}_\mu$, ν_e , and $\bar{\nu}_e$) derived in Sec. II. Equation (68) describes the average energy losses transferred to gamma rays and leptons. In order to calculate the energy losses due to pair production one should multiply Eq. (67) to $2E_e$ and integrate over dE_e .

Calculations of energy losses of protons can be performed directly, without intermediate calculations of energy distributions of secondary photons and leptons. In this regard, the energy losses of protons in 2.7 K CMBR have been studied in great detail by many authors, in particular, by Berezhinsky and coauthors [3] based on a semianalytical method of calculations and Stanev *et al.* [5] based on Monte Carlo simulations using the SOPHIA code. Therefore it is interesting to compare our results with direct calculations of energy losses. In Fig. 11 we show the

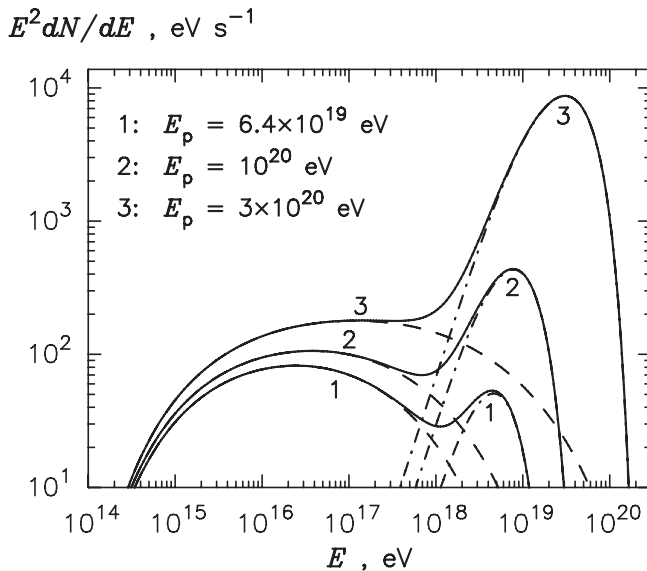


FIG. 10. Energy distributions of electrons and positrons ($N_e = N_+ + N_-$) produced at interactions of protons with 2.7 K CMBR. Dashed lines and dot-dashed lines correspond to the pair-production and photomeson processes, respectively. Solid lines show the sums of two contributions. The curves correspond to three energies of protons: 6.4×10^{19} eV, 10^{20} eV, and 3×10^{20} eV.

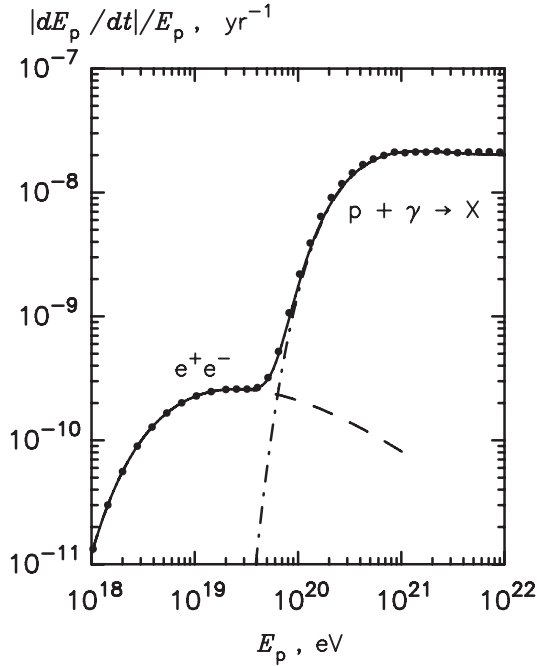


FIG. 11. The average energy loss rates of protons in the CMBR with temperature 2.726 K. The lines are obtained using our method of integration of energy spectra of all final (stable) secondaries, and the points are from [5]. They are obtained from Monte Carlo simulations of interactions of protons with the CMBR photons using the SOPHIA code. The dashed and dash-dotted lines describe the energy losses due to pair-production and photomeson interactions, respectively; the solid lines represent the sum of these two contributions.

energy loss rate of protons in the blackbody radiation field with temperature $T = 2.726$ K. For comparison, we show the result of calculations performed using the code SOPHIA [5]. The agreement of two calculations is an indirect test of a good accuracy of the above obtained approximate analytical presentations for energy distributions of stable products from proton-photon interaction.

In Fig. 12 we show the interaction rate of protons with 2.7 K CMBR, as well as the fraction of energy lost by the proton per interaction (the so-called inelasticity coefficient). Close to the threshold of pair production around $E \approx 10^{18}$ eV, $\langle x \rangle_{e^+e^-} = 2m_e/m_p \approx 1.1 \times 10^{-3}$, as it is expected from the kinematics of the process. However, with an increase of energy, $\langle x \rangle_\pi$ gradually decreases down to 10^{-4} at 10^{20} eV. This effect has also been noticed in [4,17]. In the case of photomeson production the inelasticity coefficient has a quite different behavior. At the threshold, $\langle x \rangle_\pi$ increases from the value of $m_\pi/(m_p + m_\pi) \approx 0.13$ to approximately 0.4 at energy 10^{22} eV. Therefore, despite the fact that the cross section of pair production significantly, by 2 orders of magnitude, exceeds the cross section of photomeson production, the energy losses at high energies are dominated by photomeson interactions.

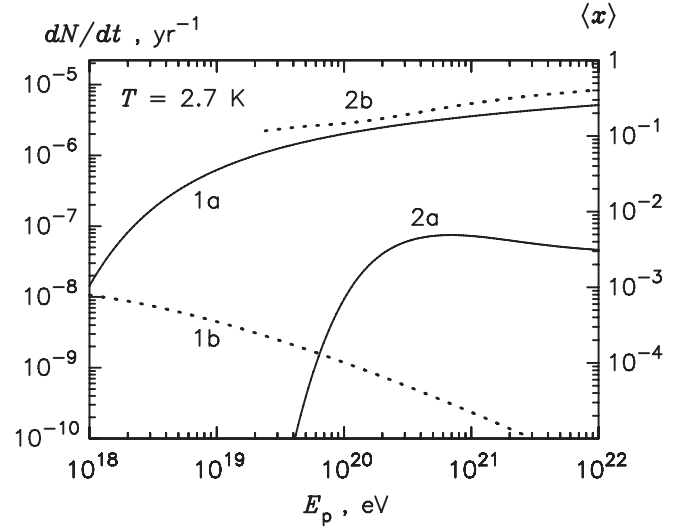


FIG. 12. The interaction rates of protons with photons of 2.7 K CMBR (left axis) and the coefficient of inelasticity (right axis). The curves 1a and 2a are the electron-positron and photomeson production rates, respectively. The curves 1b and 2b are the average energy lost by a proton of given energy due to pair production and photomeson production, respectively.

V. CALCULATIONS FOR POWER-LAW DISTRIBUTION OF PROTONS

Instead of integrating Eqs. (11) and (30) over $d\epsilon$, it is more convenient to perform integration of these equations over $d\eta$. This allows the spectra of photons and leptons to be presented in the form

$$\frac{dN}{dE} = \int_{\eta_0}^{\infty} H(\eta, E) d\eta. \quad (69)$$

Here

$$H(\eta, E) = \frac{m_p^2 c^4}{4} \int_E^{\infty} \frac{dE_p}{E_p^2} f_p(E_p) f_{\text{ph}}\left(\frac{\eta m_p^2 c^4}{4E_p}\right) \Phi\left(\eta, \frac{E}{E_p}\right), \quad (70)$$

where E is the energy of gamma rays or leptons, and Φ is the energy distribution of the given type of particle.

For photomeson interactions, it is useful to introduce the following characteristic energy of proton:

$$E_* = m_p c^2 \left(\frac{m_p c^2}{4kT} \eta_0 \right) \approx 3.0 \times 10^{20} \text{ eV}. \quad (71)$$

At energy $E_p = E_*$, the proton and a photon of energy kT can produce a pion through a head-on collision.

The function $H(\eta, E)$ at fixed energy E describes distribution over η . For a power-law distribution of protons, $f_p(E_p) \propto E_p^{-\alpha}$, the function $H(\eta, E)$ has a maximum at $\eta/\eta_0 \approx 3E/E_*$; the position of the maximum slightly depends on the power-law index α of the proton distribution. The function $H(\eta, E)$ for gamma rays is shown in Fig. 13 at $E_\gamma = 0.5E_*$ and two power-law indices, $\alpha = 2$

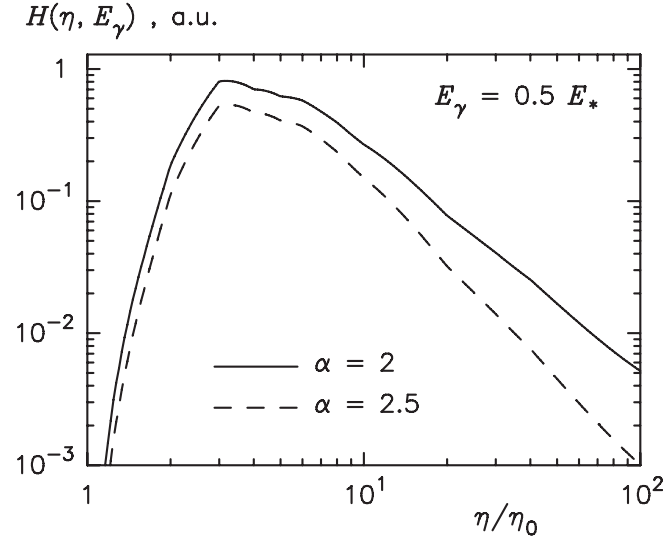


FIG. 13. Function $H(\eta, E_\gamma)$ at fixed energy of gamma rays, $E_\gamma = 1/2E_*$, calculated for a power-law distribution of protons $f_p(E_p) \propto E_p^{-\alpha}$ with $\alpha = 2$ and 2.5.

and 2.5. At low energies the function $H(\eta, E)$ drops very quickly. A cutoff in the spectrum of protons results in a faster decrease of $H(\eta, E)$ and to a shift of the point of maximum towards smaller η . For electrons and neutrinos

$H(\eta, E)$ has similar behavior—a maximum at $\eta \ll 100\eta_0$ and strong decrease with increase of η .

To use the analytical parametrizations for distributions of photons and electrons given by Eqs. (27) and (31) and related Tables I, II, and III, which are applicable for $\eta/\eta_0 \leq 100$, the following condition should be fulfilled: $3E/E_* \ll 100$. In this case the main contribution to the integral (69) comes from the region $\eta \ll 100\eta_0$, i.e., from events close to threshold. Therefore the obtained approximate analytical presentations allow calculations of distribution of particles in the energy range $E \lesssim E_*$.

Finally, let us discuss the production of photons and leptons at interactions of photons with a realistic distribution of protons, namely, a power law with an exponential cutoff:

$$f_p(E_p) = AE_p^{-2} \exp\left(-\frac{E_p}{E_{\text{cut}}}\right), \quad (72)$$

where the normalization coefficient is determined from the condition

$$\int_{1 \text{ GeV}}^{\infty} E_p J_p(E_p) dE_p = 1 \frac{\text{erg}}{\text{cm}^3}. \quad (73)$$

In Figs. 14–17 we show the spectra of photons, electrons, and neutrinos produced in photomeson interactions

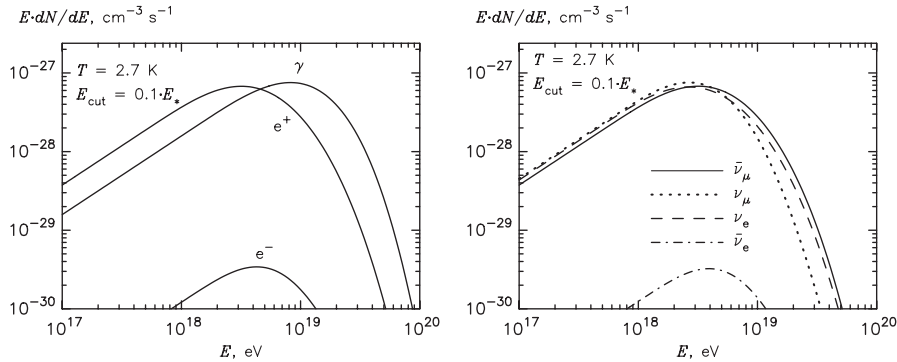


FIG. 14. The production spectra ($E dN/dE$) of photons and electrons (left panel) and neutrinos (right panel) produced with energy distribution described by Eq. (72) through the photomeson channel. The cutoff energy in the proton spectrum is assumed $E_{\text{cut}} = 0.1E_*$.

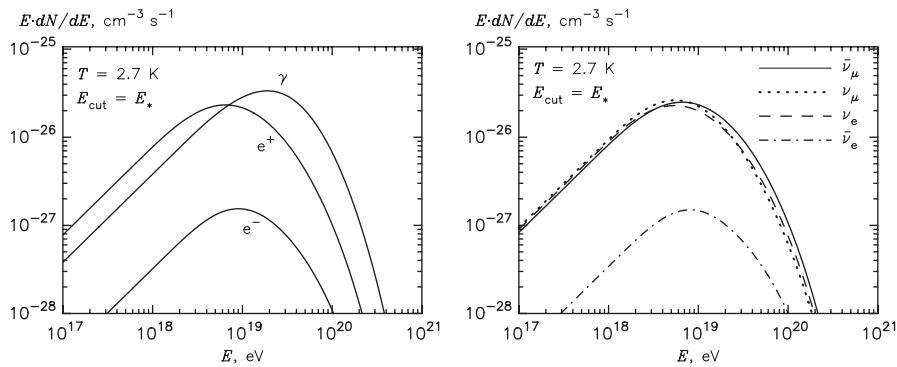


FIG. 15. The same as in Fig. 14 but for $E_{\text{cut}} = E_*$.

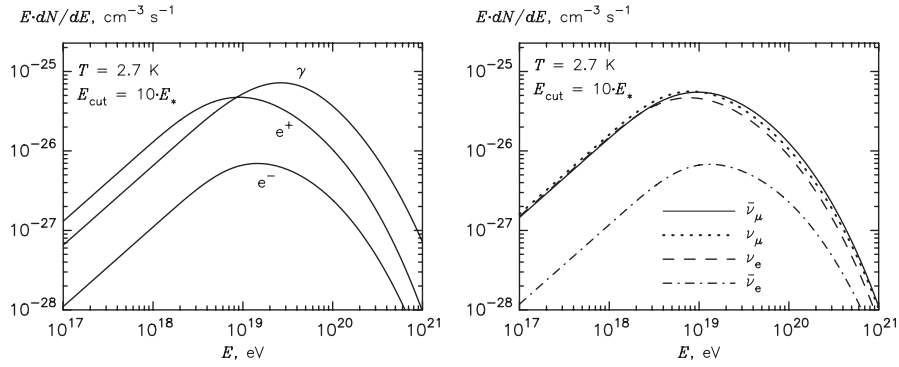


FIG. 16. The same as in Fig. 14 but for $E_{\text{cut}} = 10 \cdot E_*$.

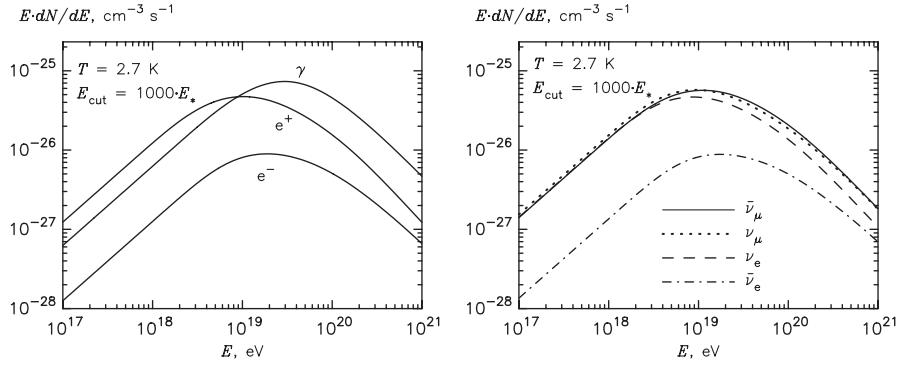


FIG. 17. The same as in Fig. 14 but for $E_{\text{cut}} = 1000 \cdot E_*$.

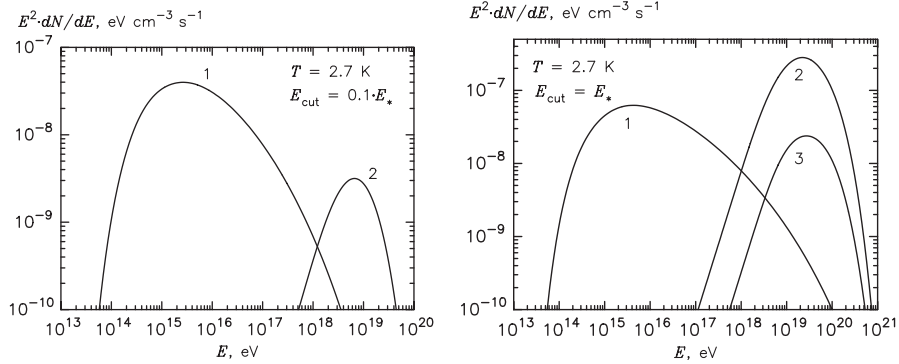


FIG. 18. The production energy spectra of electrons and positrons produced through the channel of pair production (curve 1) and positrons and electrons produced through the photomeson interactions of protons (curves 2 and 3, respectively). The proton spectrum is assumed in the form given by Eq. (72) with cutoff energy at $E_{\text{cut}} = 0.1E_*$ (left panel) and $E_{\text{cut}} = E_*$ (right panel). Note that the contribution of electrons (curve 3) in the left panel appears below the low bound of the y axis.

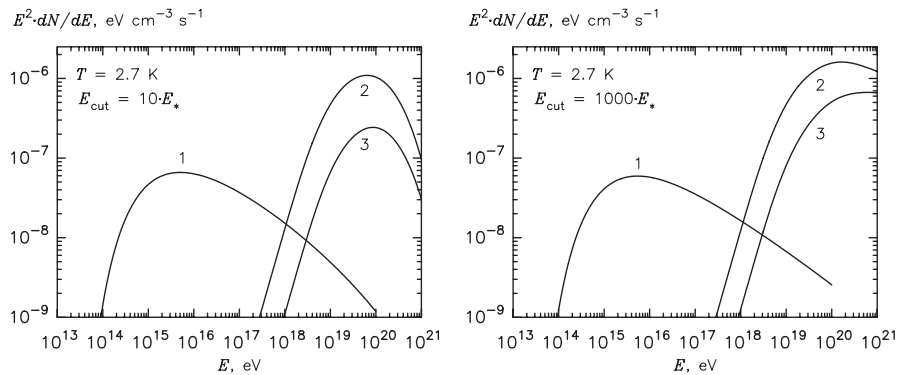


FIG. 19. The same as in Fig. 18, but for cutoff energies $E_{\text{cut}} = 10E_*$ (left panel) and $E_{\text{cut}} = 1000E_*$ (right panel).

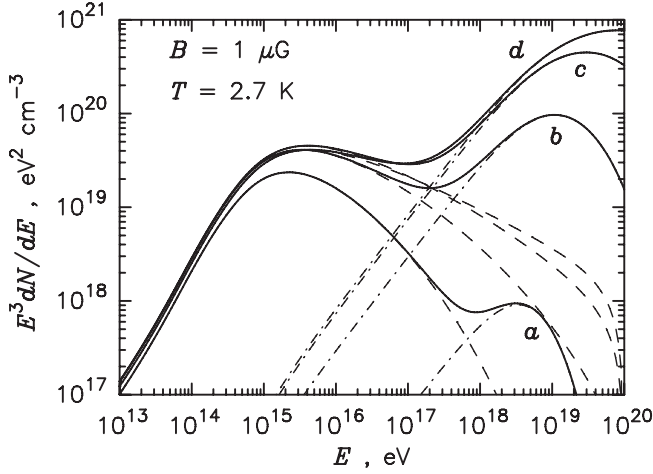


FIG. 20. The cooled spectra of electrons and positrons, $N = N_+ + N_-$. Dashed lines—electrons produced through the pair-production channel; dot-dashed lines—electrons produced through photomeson interactions. The sum of two contributions is shown by the solid curves. The proton spectrum is given in the form of Eq. (72), with $E_{\text{cut}} = 0.1 \cdot E_*$ (a), E_* (b), $10 \cdot E_*$ (c), and $1000 \cdot E_*$ (d).

calculated for four values of the cutoff energy in the proton spectrum $E_{\text{cut}} = 0.1 \cdot E_*$, E_* , $10 \cdot E_*$, and $10^3 \cdot E_*$, respectively. The case $E_{\text{cut}} = 10^3 \cdot E_*$ is almost identical to a pure power-law spectrum of protons.

In Figs. 18 and 19 we compare the spectra of electrons (and positrons) produced through the pair-production

channel with the spectra of electrons from the decay of photoproduced charged pions.

Finally, in Fig. 20, we show the steady-state spectra of cooled electrons. We assume that electrons are cooled via synchrotron radiation in the intergalactic magnetic field $B = 1 \mu\text{G}$ and inverse Compton (IC) scattering on the 2.7 K CMBR. Since the production spectrum of pair-produced electrons below $E \sim 10^{15}$ eV drops sharply (see Figs. 18 and 19), the synchrotron and IC cooling (in the Thomson regime) leads to the formation of a standard E^{-2} -type spectrum. This is clearly seen in Fig. 20.

In Fig. 21 we show the spectra of synchrotron and IC radiation of secondary electrons produced via pair-production and photomeson production channels for a fixed magnetic field of $B = 1 \mu\text{G}$, the temperature of CMBR $T = 2.7$ K, and for four different cutoff energies in the proton spectrum E_{cut} . Figure 21(a) corresponds to the cutoff energy of protons $E = 0.1 E_*$. In this case the electrons are contributed mainly from the pair-production process with a maximum in the energy distribution ($E^2 dN/dE$) at energy $E \sim 10^{15}$ eV. While synchrotron radiation of these electrons peaks at $E_\gamma \propto BE^2 \sim 10^6$ eV, the maximum of the IC radiation appears, because of the Klein-Nishina effect, at $E_\gamma \sim E_\pm \sim 10^{14}$ – 10^{15} eV. Note that although energy density of the magnetic field corresponding to $B = 1 \mu\text{G}$ is $B^2/8\pi \approx 4 \times 10^{-14}$ erg/cm³, i.e., an order of magnitude smaller than the energy density of 2.7 K CMBR, emissivity of the synchrotron and IC components are comparable. This is also a direct conse-

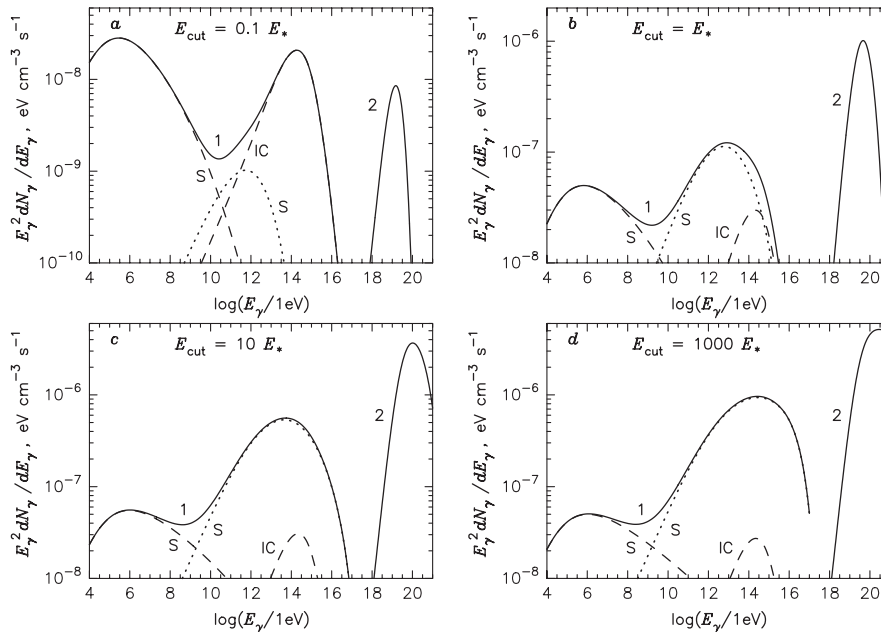


FIG. 21. The synchrotron and IC spectra of cooled electrons. Dashed lines correspond to synchrotron (S) and IC radiation of electrons and positrons produced in the pair-production process; the dotted lines correspond to radiation of positrons (electrons) produced through photomeson interactions. Curve 1 (solid lines) is the sum of these contributions. Curve 2 represents the spectrum of gamma rays produced at the decay of photoproduced π^0 mesons. The proton spectrum is given in the form of Eq. (72), with $E_{\text{cut}} = 0.1 E_*$ (a), $E_{\text{cut}} = E_*$ (b), $E_{\text{cut}} = 10 E_*$ (c), and $E_{\text{cut}} = 1000 E_*$ (d). Magnetic field $B = 1 \mu\text{G}$; temperature $T = 2.7$ K.

quence of the reduction of the cross section of IC scattering of 10^{15} eV electrons in the Klein-Nishina regime. The second component of synchrotron radiation related to the electrons from photomeson processes peaks at much higher energies, $E_\gamma \sim 10^{12}$ eV; however, its contribution is not significant because of suppression of the protons at energies above the threshold of photomeson reactions. The increase of the cutoff energy in the proton spectrum, E_{cut} , leads to dramatic orders of magnitude, increase of the emissivity of the synchrotron radiation of photomeson electrons [see Figs. 21(b)–21(d)]. At the same time, because of the Klein-Nishina cross section, only pair-produced electrons contribute to the IC radiation. Therefore the cutoff energy E_{cut} does not have any impact on the IC spectrum and emissivity, as it is seen in Figs. 21.

VI. SUMMARY

We present simple analytical parametrizations for energy distributions of photons, electrons, and neutrinos produced in interactions of relativistic protons with an isotropic monochromatic radiation field. The results on photomeson processes are obtained using numerical simulations of proton-photon interactions based on the public available Monte Carlo code SOPHIA. We also developed a simple formalism for calculations of energy spectra of electrons and positron from the pair-production (Bethe-

Heitler) process based on the well-known differential cross section in the rest frame of the proton. The energy loss rate of protons due to photomeson and pair-production processes in the 2.7 K CMBR calculated by integrating the energy distributions of the stable products of interactions is in excellent agreement with results of previous works based on direct calculations of energy losses (without an intermediate stage of energy distributions of secondaries). The analytical presentations of energy distributions of photons and leptons obtained in this paper provide a simple but accurate approach for calculations of broadband energy spectra of gamma rays, electrons, and neutrinos in different astrophysical environments.

ACKNOWLEDGMENTS

We appreciate the help of Slava Bugayov who provided us with energy distributions of secondary particles produced at photomeson interactions based on Monte Carlo simulations using the public available code SOPHIA. We thank Anita Reimer for providing us with numerical results of energy losses of protons in the 2.726K CMBR published in [5]. We thank Andrew Taylor and Mitya Khangulyan for discussion of the results. Finally we thank the referee for the constructive and very useful comments which helped us to improve the paper significantly.

-
- [1] F. W. Stecker, *Phys. Rev. Lett.* **21**, 1016 (1968).
 - [2] G. R. Blumenthal, *Phys. Rev. D* **1**, 1596 (1970).
 - [3] V. S. Berezinsky and S. I. Grigorieva, *Astron. Astrophys.* **199**, 1 (1988).
 - [4] M. Chodorowski, A. Zdziarski, and M. Sikora, *Astrophys. J.* **400**, 181 (1992).
 - [5] T. Stanev, R. Engel, A. Mücke, R. J. Protheroe, and J. P. Rachen, *Phys. Rev. D* **62**, 093005 (2000).
 - [6] A. M. Atoyan and C. D. Dermer, *Astrophys. J.* **586**, 79 (2003).
 - [7] F. A. Aharonian, *Mon. Not. R. Astron. Soc.* **332**, 215 (2002).
 - [8] S. Inoue, F. A. Aharonian, and N. Sugiyama, *Astrophys. J.* **628**, L9 (2005).
 - [9] S. Gabici and F. A. Aharonian, *Phys. Rev. Lett.* **95**, 251102 (2005).
 - [10] E. Armengaud, G. Sigl, and F. Miniati, *Phys. Rev. D* **73**, 083008 (2006).
 - [11] A. Mücke, R. Engel, J. P. Rachen, R. J. Protheroe, and T. Stanev, *Comput. Phys. Commun.* **124**, 290 (2000).
 - [12] S. R. Kelner, F. A. Aharonian, and V. V. Bugayov, *Phys. Rev. D* **74**, 034018 (2006).
 - [13] T. K. Gaisser, *Cosmic Rays and Particle Physics* (Cambridge University Press, Cambridge, England, 1990).
 - [14] P. S. Coppi and F. A. Ahronian, *Astrophys. J.* **487**, L9 (1997).
 - [15] R. L. Gluckstern, M. H. Hull, and G. Breit, *Phys. Rev.* **90**, 1026 (1953).
 - [16] R. L. Gluckstern and M. H. Hull, *Phys. Rev.* **90**, 1030 (1953).
 - [17] A. Mastichiadis, R. J. Protheroe, and J. G. Kirk, *Astron. Astrophys.* **433**, 765 (2005).